The princess and the pea: seasonal development of the desmid *Oocardium stratum* along a limestone-precipitating spring stream

Caroline Linhart & Michael Schagerl

View supplementary material

Published online: 27 Sep 2019.

Submit your article to this journal

Article views: 416

View related articles

View Crossmark data

International Phycological Society

Taylor & Francis
Taylor & Francis Group

🔓 OPEN ACCESS ✓ Check for updates

The princess and the pea: seasonal development of the desmid *Oocardium stratum* along a limestone-precipitating spring stream

Caroline Linhart[1]* and Michael Schagerl[2]*

[1]Institute of Pharmacy/Pharmaceutical Chemistry and Center for Molecular Biosciences Innsbruck (CMBI), University of Innsbruck, Innrain 80-82, A-6020 Innsbruck, Austria
[2]Department of Limnology and Bio-Oceanography, University of Vienna, Althanstraße 14, Vienna A-1090, Austria

ABSTRACT

The desmid *Oocardium stratum* is restricted to short sections of active limestone-precipitating springs (LPS) and adjacent headstreams. We studied the succession of photoautotrophic biofilms on artificial substrate at three sites in an LPS stream in spring, summer and autumn. We exposed frosted glass slides between 3 and 12 weeks, and measured calcium carbonate precipitation (CCP), nutrients and environmental parameters. Relative amounts of *O. stratum*, Bacillariophyceae and Cyanobacteria to overall biomass of the photoautotrophic biofilm were estimated by means of class-specific photosynthetic pigments. Overall, 77% of the photoautotrophic biomass consisted of diatoms, 20% were related to *O. stratum* and 3% were related to Cyanobacteria. Biomass of *O. stratum* and diatoms showed a significant correlation with CCP ($r = 0.61$ and 0.46), while for Cyanobacteria there was no significant correlation. CCP increased exponentially over time and peaked in late summer and late autumn (maximum CCP measured as ash mass was around 10 µg mm^{-2} week^{-1}). We applied generalised multiple linear regression models (GLM) to evaluate the influence of stream site, weeks of exposure, season and CCP on biofilm development. According to GLM, the biomass of *O. stratum* was associated with site, exposure time, season and CCP, while the biomass of Cyanobacteria and Bacillariophyceae were not associated with the input variables. The negative standardised beta coefficient of cyanobacterial biomass in the multivariate regression model for the biomass of *O. stratum* suggest a competition between the two taxa. This likely explains the restricted occurrence of *O. stratum* within a short section of the active LPS stream.

INTRODUCTION

Carbonate precipitation due to biomineralisation occurs in the sea, in inland waters and soils (Martinez *et al.* 2010). Pelagic marine microorganisms have the greatest impacts on carbonate sedimentation (Field 1998; Martinez *et al.* 2010) and marine animals and seaweeds contributed to mountain formation, such as the Dolomite Alps (Bosellini *et al.* 2003; Faupl 2003). Besides macrophytes and animals, biomineralisation in inland waters is caused by microbial mats, which control mainly the equilibrium between organic and inorganic carbon (Dupraz *et al.* 2009). A clear distinction between biogenic- and abiogenic-induced calcium carbonate precipitation (CCP) is not always obvious (Merz-Preiß & Riding 1999), especially if the deposition is linked to Cyanobacteria or microalgae such as the desmid *Oocardium stratum* Nägeli. Dupraz *et al.* (2009) listed three different types of biomineralisation processes: biologically induced (Bazylinski 2003; Weiner 2003), biologically controlled, and biologically influenced mineralisation. Additionally, $CaCO_3$ deposition, exclusively related to abiotic processes such as reduced solubility of CO_2 due to heating and/or atmospheric degassing of CO_2 from supersaturated groundwater, occurs in aquatic habitats.

In active limestone-precipitating springs (LPS; Cantonati *et al.* 2016) and adjacent headwaters, $CaCO_3$ precipitates on any available surface, a condition which was termed by Sanders *et al.* (2010) as spring-associated limestone (SAL). Meteogene calcium carbonate is formed due to degassing of supersaturated carbon dioxide originating from soil and root respiration, which was originally fixed from the atmosphere. According to Pentecost (2005, 1991), the mean deposition rate of meteogene limestone is around 5 mm yr^{-1}, and may increase to 9 mm yr^{-1} when eukaryotic algae are involved to a greater extent. CCP rates of 2.2 mm yr^{-1} for LPS streams with Cyanobacteria were observed by Merz-Preiß & Riding (1999).

Oocardium stratum is found exclusively in active meteogene LPS with ambient water temperature, and growing on various surfaces encrusted with SAL. Cells resemble those of *Cosmarium* and *Cosmocladium* (width 15–20 µm, length 10–20 µm) and are located at the ends of gelatinous stalks encrusted with carbonate (Golubić & Marčenko 1958; Linhart & Schagerl 2015; Sanders & Rott 2009; Schagerl & Pröschold 2007; Wallner 1933, 1934). The stalk system consists of extracellular polymeric substances, and proved to be an ideal

nucleation site for CCP (Pentecost 1985). 'Oocardium tufa' is even known from rock formations. Wallner (1935) reported a deposition rate of 5 mm a^{-1} in thickness for *Oocardium*-associated limestone. Studies focusing on formation and lamination induced by *O. stratum* have been carried out by Sanders & Rott (2009) and by Trobej *et al.* (2017), who measured deposition rates in the presence of *O. stratum* between 1 and 10 mm yr^{-1}. It still remains unclear if *O. stratum* shows influenced, controlled or induced biomineralisation (Pentecost 1991; Rott *et al.* 2010; Sanders & Rott 2009; Wallner 1934).

The few studies of this peculiar taxon focused mainly on SAL formation, and ecological demands of *O. stratum* were largely neglected. Sanders & Rott (2009) suggested that seasonal changes in irradiance supply control the occurrence of *O. stratum*, resulting in SAL lamination. CCP was high during warmer periods (up to 5 mm), coinciding with intense growth of *O. stratum*, followed by a strong reduction caused by the massive development of benthic diatoms during autumn and winter, with only a few colonies of *O. stratum* persisting during the cold season. Linhart & Schagerl (2015) identified hydrogen carbonate and water temperature as key variables for growth of *O. stratum* in a small LPS stream. In comparison with LPS, Trobej *et al.* (2017) found *O. stratum* exclusively at higher CCP rates linked to soluble reactive phosphorus concentrations below 3 µg l^{-1}.

The current study focused on the succession of photoautotrophic biofilms in an LPS stream. Specifically, we evaluated key parameters responsible for the development of *O. stratum*. Factors could be either biotic interactions, i.e. competition, grazing and/or environmental factors such as CCP, nutrients and/or specific physical conditions. We hypothesised that higher *O. stratum* growth during summer is caused mainly by increased incoming irradiance and warmer temperature. We also assumed that *O. stratum* was dominant during periods of increased CCP, which can be seen as a competitive benefit in such environments.

MATERIAL AND METHODS

Study site

We studied a small LPS stream discharging into the Mayrbach, which is located in the south-west faced slope of the Mayrgraben system in Lunz am See (47°15′ N, 15°04′ E; 714 m above sea level). The area is part of the limestone alps of Lower Austria (Fig. 1). Bedrock of the Mayrgraben system is a sandstone and shale formation of the Lunzer beds. The riparian vegetation consists of annual herbs, e.g. *Fraxinus excelsior* Linnaeus, *Fagus sylvatica* Linnaeus, *Picea abies* Karst, and *Rubus* subgen. *rubus* Linnaeus. Mean annual precipitation is about 1740 mm yr^{-1} and the mean annual air temperature is 7.4 °C. After a heavy storm event in 2007 (winter storm 'Kyrill', January 2007), most SAL layers were destroyed, leading to a collapse of the *O. stratum* population. This disturbance provided the opportunity to study the succession of the system including recolonisation of *O. stratum*. The three study sites were located along the LPS stream (Fig. 1), which can be characterized as a spring system of small diffuse helocrenes with the adjacent headwater (Vannote *et al.* 1980) of stream order 1 of the Strahler system (Strahler 1957). Site S was located next to the spring; here, SAL deposition starts. This site was also characterised by high incident irradiance. Site C was located about 25 m downstream in the centre of the LPS stream stretch; artificial shading was constructed at this site to mimic former canopy cover. Site M was located 10 m downstream towards the mouth of the LPS stream, where it discharges into the Mayrbach. This site is also characterised by high irradiance; it is located on an SAL cascade.
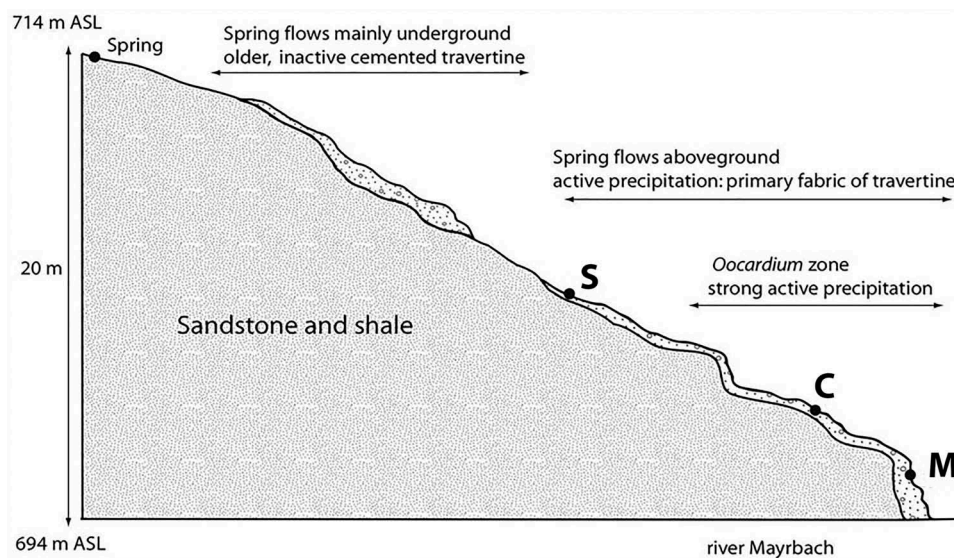
Fig. 1. Altitude profile of study site with locations of sampling sites S, C, and M. The spring of the *Oocardium* headwater is 714 m above sea level. After a few m aboveground, the headwater flows mostly underground. Inactive and cemented travertine indicates the former spring course. At an altitude of 703 m above sea level, the rivulet again flows aboveground and active precipitation starts. The *Oocardium* zone starts 65 m downstream of the spring and ends after 84 m.

Experimental set-up and data collection

The study took place between March 2008 and July 2009. We collected water samples in weekly intervals from March 2008 to November 2008, and from April 2009 to July 2009. Sampling was not possible in the winter season due to snow cover > 1 m. At each site, a set of environmental data was collected according to standard procedures (Linhart & Schagerl 2015; for an overview of methods see Table S1).

We installed sets of 25 frosted glass slides fixed in acrylic glass frames at each of the sites S, C and M. Frames were mounted on the limestone surface so that the slides were submerged in stream water. Slides were combusted before exposure (450 °C, 4 h) and then handled only with rubber gloves. Slides were exposed from 2 to 12 weeks to observe the initial state of carbonate precipitation, and to measure CCP rate, algal biomass and algal community composition. Slides were placed *in situ* on 15 July 2008, and the last retrieval was on 15 November. Slides were exposed again between 7 April and 30 June 2009. Every 2 weeks, five slides were randomly replaced, in order to collect carbonate and biomass samples.

For analysis, slides were carefully removed from the glass frames and transported in sterile 50-ml centrifuge tubes to the nearby laboratory. The cover was scraped with a scalpel and rinsed back into the tubes. In order to determine CCP rate, and levels of chlorophyll *a* (Chl*a*) and accessory pigments, samples were homogenised (PT 1600 E disperser) and separated into subsamples. Subsamples were gently vacuum filtered on precombusted and pre-weighted glass fibre filters (Whatman GF/F, GE Healthcare, Chicago, Illinois, USA). One set of subsamples was subsequently oven-dried (90 °C, 24 h), weighed for dry mass (DM) and incinerated (450 °C, 4 h) to determine ash mass (AM) and to calculate particulate organic matter (POM = DM – AM). AM was treated as CCP. We analysed AM samples with X-ray diffraction (XRD) in order to determine mineral fractions of the precipitate.

Filters for pigment analysis were kept frozen at −80 °C until extraction, which took place in the Vienna laboratory. Filters were ground in 90% acetone and the extract stored in the dark for 8 h in a refrigerator (4 °C). After centrifugation (15 min, $1000 \times g$, 10 °C), the supernatant was analysed using high performance liquid chromatography (HPLC system Hitachi Elite LaChrom, Diode Array Detector Hitachi L-2455, column thermostat L-2300 with temperature of 35 °C, column Superspher RP–18, 100 LIChrocart, pre-column LIChrocart rP-18 end-capped, peak integration with EZChrom Elite Client Version 3.2) according to a modified protocol of Wright *et al.* (1991). Peaks were quantified at 440 nm and identified by comparing retention times, absorption peaks and co-chromatography with authentic standards (DHI Bioproducts, Hørsholm, Denmark). In order to determine the percentages of *O. stratum* (the dominating streptophyte), Bacillariophyceae, and Cyanobacteria in samples, we first had to evaluate class-specific pigment ratios (Table S2). For *O. stratum* we used species-specific pigment ratios of clonal cultures, and for Bacillariophyceae and Cyanobacteria we took the average of class-specific pigment ratios from literature

(Brotas & Plante-Cuny 2003; Mackey *et al.* 1997; Schagerl & Donabaum 2003; Schlüter *et al.* 2000). Both the pigment ratio matrix and the field-sample matrix were taken as input data to estimate algal class abundance relative to Chl*a* as a surrogate for total algal biomass (see data analysis). Chl*a* was also measured spectrophotometrically (see Talling & Driver 1963) and this served as a control for HPLC pigment analyses. Qualitative observations of the biofilm were performed with a confocal laser scanning microscope (Zeiss LSM710, Zeiss, Oberkochen, Germany) and a Zeiss Axio Imager.M1 compound microscope (camera: Axio Cam MRc5, computer application: Axio Vision Release 4.7.2).

Data analysis

Data analysis was done using R statistical software v3.5.1 (R Core Team 2018). Continuous variables were presented as medians with interquartile range (IQR) and categorical variables as percentages. Data were first tested for normal distribution using the Kolmogorov–Smirnov test. Non-normally distributed data such as environmental data, biomass (Chl*a* ng mm^{-2}), CCP (μg mm^{-2}), and community composition were transformed with y = $\log_{10}(x + 1)$ function (Burns & Walker 2000; Ramette 2007) to achieve normality.

Two-way ANOVA followed by a *post hoc* test (Tukey test) was used to compare environmental factors between the three sites and three seasons. Correction for multiple testing (*post hoc* tests and Welch correction) was applied where necessary. Community composition by means of HPLC data was performed with BCE, (Bayesian compositional estimator; Van Den Meersche *et al.* 2008). Descriptive statistics, correlation, regression analysis and graphical prediction analysis were performed with jtools, ggpubr, ggplot2 and apaTables.

For correlation, regression and prediction analysis, data were standardised to zero mean and unit variance. First, Pearson's bivariate correlations were performed on transformed CCP and biomass data. Then, a multivariate generalised linear regression model (GLM) was performed to identify the impact of site-related factors, exposure time, season and CCP on biomass data of *O. stratum*, Bacillariophyceae and Cyanobacteria (GLM1). We used 'site' as an independent factor representing the downstream gradient in water chemistry while the factor 'season' characterised changes over the year of water temperature, radiation and sky openness. We additionally calculated a GLM2 with only *O. stratum* biomass as a dependent variable to consider impacts of both abiotic factors and biotic interactions with other photoautotrophs on *O.stratum* biomass. Model evaluation and test for over-dispersion were done by the analysis of deviance using the anova() function. Homoscedasticity of the models was confirmed using the Breusch–Pagan test (Breusch & Pagan 1979). Model evaluation and the final selection were based on comparisons of r^2, adjusted r^2, AIC and BIC (Zuur *et al.* 2009). We considered $P < 0.05$ as statistically significant. Biomass was predicted graphically over time with the function geom_smooth in the ggplot package, providing a LOESS function to model untransformed data of a polynomial surface through the local fitting.

RESULTS

Environmental parameters

Water temperature ranged from 3.6 °C to 16.1 °C with a mean ($\bar{x}$) of 10.7 °C (standard deviation, s = 2.9). Sky openness ranged from 13.9% to 48.8% with a mean of 30.9% (s = 8.9); pH was slightly alkaline (8.1–8.4). Ca^{2+} was the dominant cation ranging from 54.1 to 92.7 mg l^{-1} with a mean of 79.8 (s = 6.1). K^+ and Na^+ were less than 1 mg l^{-1}. Free carbon dioxide ranged from 0.8 to 4.8 mg l^{-1} with a mean of 2.2 mg l^{-1} (s = 9.4). HCO_3^- was the dominant anion with a mean of 4.4 mg l^{-1} (s = 0.3) followed by SO_4^{3-} ($\bar{x}$ =2.8 mg l^{-1}, s = 0.3) and Cl^- (0.3 to 0.9 mg l^{-1}). Nutrient levels were generally low; soluble reactive phosphorus was below 3.6 µg l^{-1} with a mean of 0.7 µg l^{-1} (s = 0.8; Tables S3, S4).

Water chemistry (ions and nutrients), irradiance, water temperature and discharge differed significantly by season (Table S4, top). The factor site is reflected mainly through differences of variables involved in the carbonate equilibria. Downstream we found a significant decline of free carbon dioxide, HCO_3^- and conductivity ($P < 0.001$). Also, sky openness differed significantly among sites ($P < 0.001$), but incoming irradiance did not ($P = 0.091$). Moreover, a significant downstream gradient was obtained for $N\text{-}NH_4$ ($P = 0.023$), but seasonal differences were higher than site-specific differences (Table S4, bottom).

CCP development

XRD showed the same mineral fractions for all AM samples: calcite (60%), aragonite (39%), and also low amounts of quartz (1%); crystal diameter was about 10 µm (Figs 9–15). In both years, CCP was not detectable in the initial 2 weeks of exposure. The lowest CCP was detected at site S in spring (0.02 µg mm^{-2}; Fig. 2), the maximum was measured at site M in autumn (116.7 µg mm^{-2}; Fig. 3). At all sites CCP precipitation started slowly in spring, but increased exponentially at sites C and M until late summer. After reaching a maximum in late summer, CCP decreased at sites C and M in early autumn but showed a strong increase in late autumn. In contrast, CCP at site S increased slightly throughout the study period with no decline in early autumn (Fig. 3). CCP indicated significant differences within sites ($F_{(2,132)} = 37.68$, $P < 0.001$) and seasons ($F_{(2,132)} = 99.93$, $P < 0.001$). It was significantly lower at site S compared to sites C and M (post hoc Tukey test; $P < 0.002$), but CCP did not differ from the more downstream sites C and M (post hoc Tukey test; $P < 0.915$). CCP was significantly lower during spring than in summer and autumn at all three sites (post hoc Tukey test; $P < 0.001$).

Furthermore, CCP displayed a strong and positive correlation with biomass of O. stratum ($r_{(135)}= 0.61$, $P < 0.001$), whereas Bacillariophyceae were only weakly correlated with CCP ($r_{(135)} = 0.46$, $P < 0.001$); cyanobacteria showed no zero-order correlation to CCP ($r_{(135)} = 0.12$, $P = 0.172$, Table S5). CCP rates ranged from 0.01 µg mm^{-2} $week^{-1}$ measured at site S in spring 2009 to 9.80 µg mm^{-2} $week^{-1}$ at site C in summer 2008 (Figs 2, 3).

PHOTOAUTOTROPHIC BIOFILM SUCCESSION

Chl$a$ was not detectable in the first 3 weeks of exposure in summer and autumn 2008, nor in spring 2009. Chl$a$ ranged
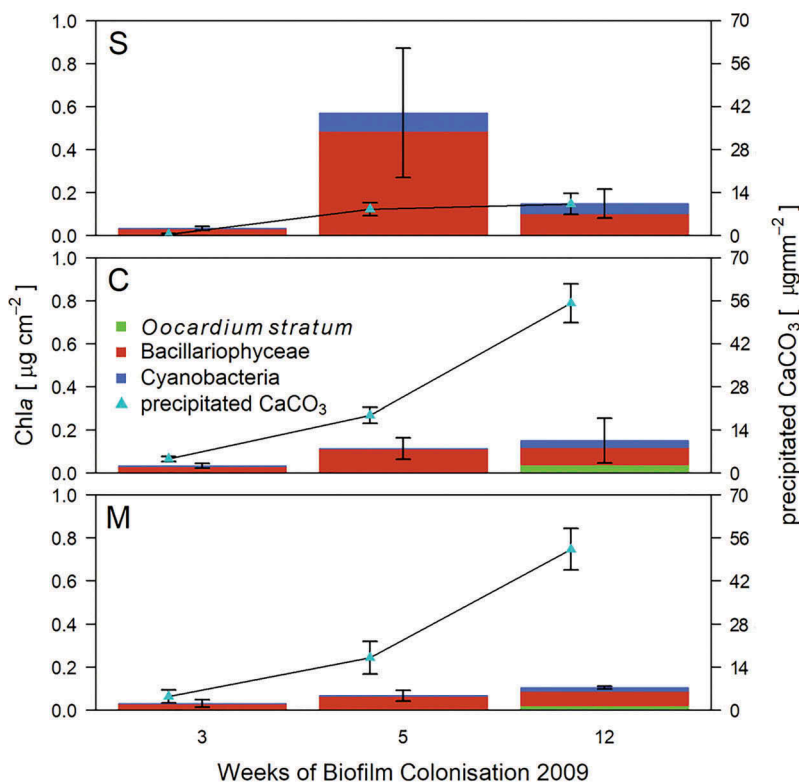

Fig. 2. Biofilm development on artificial substrata (frosted glass slides) along headwater for sites S (spring), C (centre) and M (stream mouth) from April to July 2009 (mean ± s).
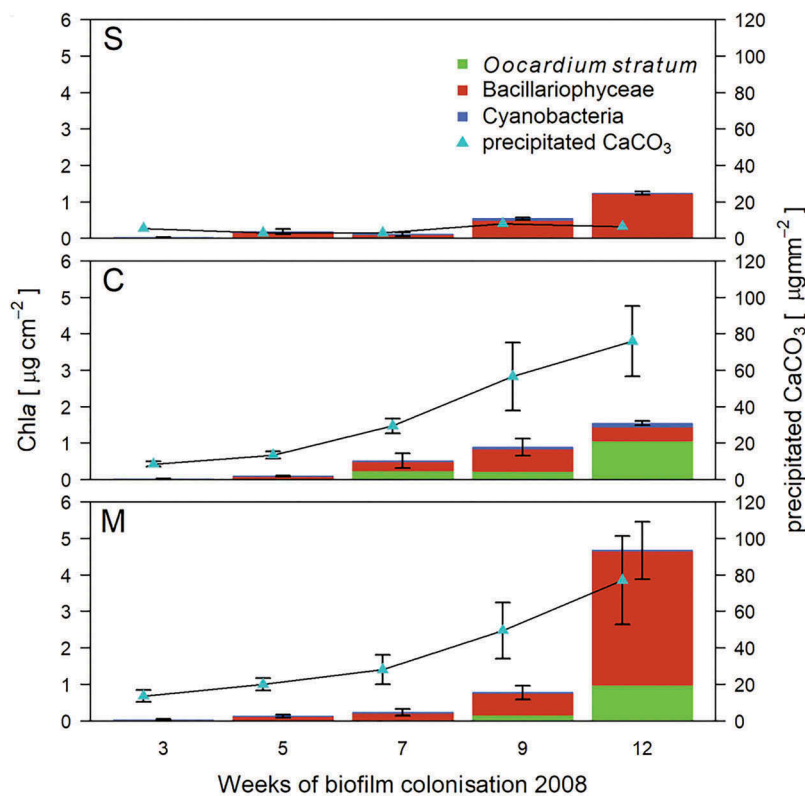
Fig. 3. Biofilm development on artificial substrata (frosted glass slides) along the headwater for sites S (spring), C (centre) and M (stream mouth) from July to November 2008 (12 weeks) (mean ± *s*).

from 0.04 µg cm^{-2} (site C) in summer to 5.55 µg cm^{-2} (M) in autumn (Figs 2, 3). Diatoms were dominated by a brownish mucous-like coating of *Encyonema minutum* (Hilse) D.G. Mann. For Cyanobacteria, only small *Synechococcus*-like forms were observed, while filamentous taxa were absent (Fig. 5). Diatoms comprised the most abundant biofilm fraction, at 28%–98% of algal biomass (Figs 2–4). However, in late summer, *O. stratum* caught up, and towards late autumn even exceeded Bacillariophyceae (Figs 3, 12–15). On average, *O. stratum* contributed 11% of total Chl*a* (range 0.1–92.8%). Cyanobacteria were never the most abundant photoautotrophs ($\bar{x}$ = 4.3%, 0.1–33.0%).

Early colonists were diatoms, followed by Cyanobacteria and finally *O. stratum* (Figs 4–20). Isolated cells of *O. stratum* were observed at C and M after 5 weeks; colonies formed after 7 weeks (Figs 9–15). Site S showed a delayed occurrence of *O. stratum*. Single cells were visible after 7 weeks followed by colony formation after 9 weeks (Figs 4–8). Growth of *Oocardium* occurred in two maxima during late summer and late autumn at sites C and M; S had only a small increase in biomass in autumn. Cyanobacteria reached a maximum in spring after 5 weeks at site S, while *O. stratum* peaked after 12 weeks at site C. Diatom biomass also reached its maximum after 12 weeks at site M.

At site S, Cyanobacteria showed significantly higher biomass than *O. stratum* ($F_{(2,132)}$ = 13.01, *P* = 0.001). Biomass of *O. stratum* was lowest at site S and higher at C and M ($F_{(2,132)}$ = 13.01, S-C: *P* < 0.001, S-M: *P* < .034). Occurrence followed an unimodal distribution (Figs 2, 3) with maximum occurrence at site C; sites S and M did not differ in biomass of *Oocardium* ($F_{(2,132)}$ = 13.01, *P* < 0.401).

GLM1 revealed that the factors: site, exposure time, season and CCP, were significantly associated with biomass of *O. stratum* and explained 58% of its growth (r^2 = 0.58, *P* < 0.001). A positive association was found with season and CCP, while the factors site and exposure time showed a significant negative association. Diatom biomass was positively associated with exposure time and CCP (R^2 = 0.38, *P* < 0.001).

The multivariate model (GLM1) further showed that season and CCP were positively associated with Cyanobacteria biomass, while the factor site showed a negative association (r^2 = 0.24; *P* < 0.001; Table S5).

GLM2, focusing on the biomass of *O. stratum*, confirmed the significant impact (*P* < .001) of site, exposure time, season and CCP. Furthermore, cyanobacteria biomass was significantly and negatively linked to *O. stratum* (*P* < 0.001, Table S6). The model explained 63% of *O. stratum* occurrence.

DISCUSSION

Biofilm development started with diatoms and an initial carbonate layer paired with Cyanobacteria, which was then replaced by *O. stratum*. Lamination of SAL developed through alteration of biofilm composition from thick diatom mats and calcified stalks of *O. stratum*. Community shifts were caused by seasonal changes. We assumed that CCP was mainly of abiotic origin, but it was also promoted by increased excretion of extracellular polymeric substances, because of the larger surface area.
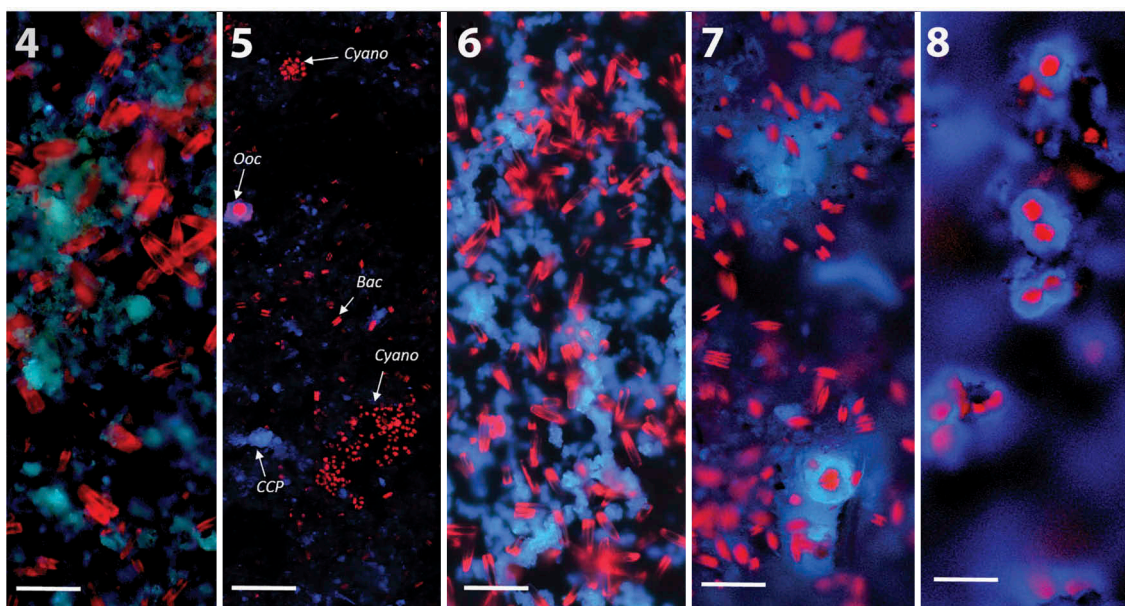
Figs 4–8. Composite three-colour CLSM images of glass slides in summer at site S showing autofluorescence of photosynthetic microorganisms and polarised CCP under 405 nm. Abbreviations: *Ooc, Oocardium stratum; Cyano*, cyanobacteria; *Bac*, diatoms.
    Fig. 4. Auto-fluorescence of initial diatoms (red) and CCP after 3 weeks (mean thickness of biofilm: 30 μm, range: 8–54 μm).
    Fig. 5. First cell of *O. stratum* (red, larger cell surrounded by calcified EPS in blue) plus cyanobacterial colonies visible after 5 weeks.
    Fig. 6. Same slide but other spot: development of a more solid carbonate layer (blue) and increase in diatom biomass after 5 weeks (mean thickness of biofilm: 60 μm, range: 15–150 μm).
    Fig. 7. Single cells of *O. stratum* with calcified gelatinous stalk surrounded by diatoms after 7 weeks (mean thickness of biofilm: 90 μm, range: 20–230 μm).
    Fig. 8. Colonies of *O. stratum* after 9 weeks beneath diatoms and cyanobacteria, which occurred at deeper levels of highly structured CCP architecture (mean thickness of biofilm: 150 μm, range: 60–300 μm. Scale bar: 50 μm).

This study revealed new and interesting patterns of photo-autotrophic biofilm succession of the dominant groups Bacillariophyceae, Cyanobacteria and Streptophyta, the latter represented by only *O. stratum*. Chl*a* amounts were comparable to Domozych & Domozych (2008), who focused on freshwater biofilms comprising desmids grown on artificial substrate. High CCP and comparably low nutrient availability might explain the low periphyton cover than in other forest streams, which usually show a tenfold higher biomass (Roberts *et al.* 2004; Sabater *et al.* 1998). Discharges of around 6 l s^{-1} after snowmelt and after heavy rains, paired with water temperature below 10 °C until the end of May, likely caused a delay of biofilm development.

Proportions of green algae, diatoms and Cyanobacteria were comparable to former studies on epilithic biofilms in alpine regions, with diatoms being the dominant photosynthetic group followed by Cyanobacteria and green algae (Zancarini *et al.* 2017). We observed an initial colonisation by diatoms and cyanobacteria; *O. stratum* growth was delayed (Figs 4–5, 9–11). We assume that extracellular polymeric substances excreted by pioneer microorganisms, i.e. beta proteobacteria and certain diatoms, have a fundamental function in biofilm succession, as this was shown in other stream systems (Battin *et al.* 2003; Besemer *et al.* 2007; Stolz 2000; Zancarini *et al.* 2017). These initial colonisers provide a matrix for subsequent organisms (Roeselers *et al.* 2007; Zancarini *et al.* 2017). Although cyanobacteria were only a minor fraction of the biofilm community, they probably play a pivotal role in initial colonisation of *O. stratum* (Figs 9–15). This process is reflected in the results of GLM2, which showed a significant negative association

between Cyanobacteria and biomass of *O. stratum* (Table S6). Cyanobacterial, extracellular, polymeric substances provide a possible explanation. According to Dupraz *et al.* (2009), cyanobacteria can influence initial CCP, especially at pH levels below 7, where negatively charged groups within the matrix of extracellular polymeric substances of picocyanobacterial origin, such as carboxylic acids and hydroxyl groups, bind large amounts of cations. As bound Ca^{2+} is removed from the running water, it leads to reduced precipitation (Dittrich & Sibler 2010; Dupraz *et al.* 2009; Zhu & Dittrich 2016). We likely observed this phenomenon (Figs 4–8, 19), especially at site S during spring, when pH was significantly lower than at sites C and M. We assume that primary CCP inhibition caused by Cyanobacteria and/or physical conditions (e.g. degassing of supersaturated carbon dioxide increased downstream) delayed colonisation of *O. stratum* (Figs 4–8, 12–15).

After about 5 to 7 weeks, cyanobacteria were outcompeted by *O. stratum*. We observed characteristic green pinhead-like colonies after 2 months of exposure in summer. High occurrence of *O. stratum* in summer was also observed by Trobej *et al.* (2017), who studied Austrian LPS streams. After settling, *O. stratum* takes the major role of 'biofilm architect' along a certain SPL stream stretch due to its high excretion of extracellular polymeric substances. This is a strategy to escape being buried in carbonate.

The occurrence of *O. stratum* was linked to the warmer season, site and CCP (highest at station C). The factor season represents mainly increased water temperature, light supply, nutrient availability, and decreased discharge. We assume that discharge is the background variable for both water
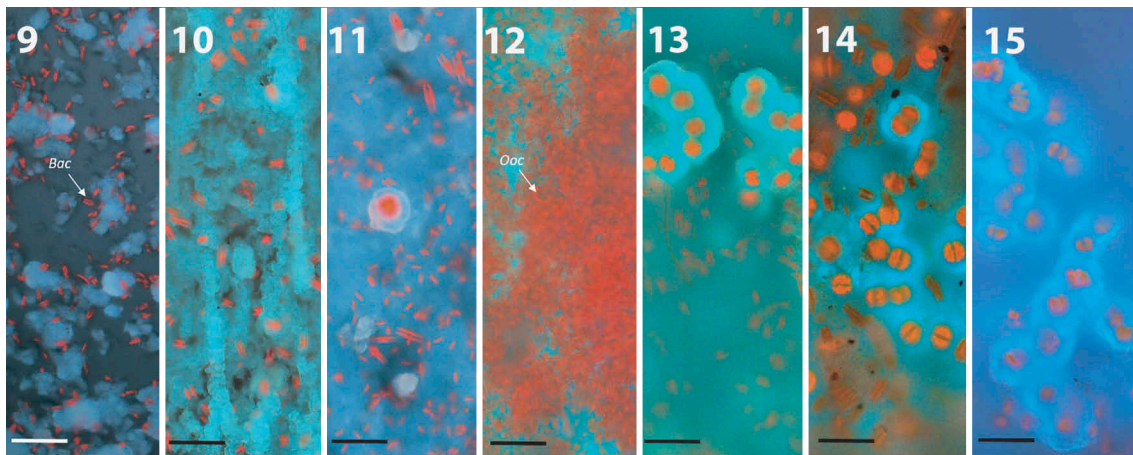
Figs 9–15. Composite three-colour CLSM images of glass slides from summer 2008 at site C showing autofluorescence of photosynthetic microorganisms and polarised CCP under 405 nm. Scale bar: 50 μm. Abbreviations: *Ooc, Oocardium stratum; Bac,* diatoms.

  Fig. 9. Auto-florescence of initial diatoms (red) and CCP after 3 weeks (mean thickness of biofilm: 56 μm, range: 15–170 μm).

  Figs 10–11. Development of a solid carbonate layer after 5 weeks (blue) shaped by stream flow. Single diatom (11) cells and (12) first single *O. stratum* cells with calcified EPS stalks on the top of the calcium carbonate layer (mean thickness of biofilm: 134 μm, range: 20–240 μm).

  Fig. 12. Thick diatom mat developed after 7 weeks on solid CCP layer (mean thickness of biofilm: 190 μm, range: 70–400 μm).

  Fig. 13. Colonies of *O. stratum* developed beneath first collapsing diatom mats after 7 weeks. Diatoms were observed also in deeper levels of the highly structured CCP architecture (mean thickness of biofilm: 280 μm, range: 110– 450 μm).

  Figs 14–15. In November 2008, after 12 weeks, diatom mats collapsed, and colonies of *O. stratum* increased. Biomass of *O. stratum* exceeded the biomass of diatoms (mean thickness of biofilm: 580 μm, range: 200–2400 μm).

temperature and nutrient availability, and is highly dependent on melting water during spring, and occasionally high current velocity after heavy rainfall. Main variables characterising the factor site are free carbon dioxide, and sky openness (both of which increased close to the spring, Tables S3, S4).

 Biomass of *O. stratum* was much more sensitive to environmental conditions than were diatoms and cyano-bacteria, which was studied by Trobej *et al.* (2017). In our study, a similar pattern was observed for *O. stratum* indicating its very site-specific preferences along the LPS stream, which merges into the Mayerbach. Although the Mayerbach offers only slightly increased nutrient levels and lower CCP, *Oocardium* was not observed there (Linhart & Schagerl 2015). The taxon can persist only in small sections, where its growth habit provides a competitive advantage.
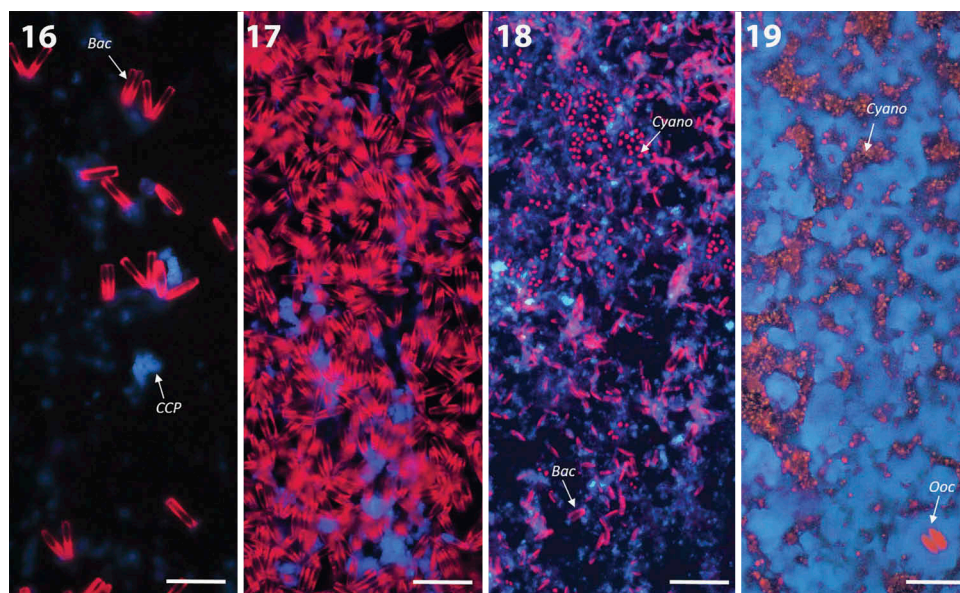
Figs 16–19. Composite three-colour CLSM images of glass slides of the growth experiment in spring at site C showing autofluorescence of photosynthetic microorganisms and polarised CCP under 405 nm. Scale bar: 50 μm. Abbreviations: *Ooc, Oocardium stratum; Cyano,* cyanobacteria; *Bac*, diatoms.

  Fig. 16. First diatoms (red) and first single calcium carbonate crystals (blue) are visible after 3 weeks (mean thickness of biofilm: 55 μm, range: 20–85 μm).

  Fig. 17. Diatom mat developed after 5 weeks (mean thickness of biofilm: 70 μm, range: 15–150 μm).

  Fig. 18. Diatom mats collapsed after 12 weeks, followed by rising of cyanobacterial colonies and formation of fine carbonate layer (blue).

  Fig. 19. Same slide but other spot: The base of the biofilm consisted of a homogenous cyanobacterial mat. First single cells of *O. stratum* occurred on more homogeneous CCP layer (mean thickness of biofilm: 155 μm, range: 15–210 μm).
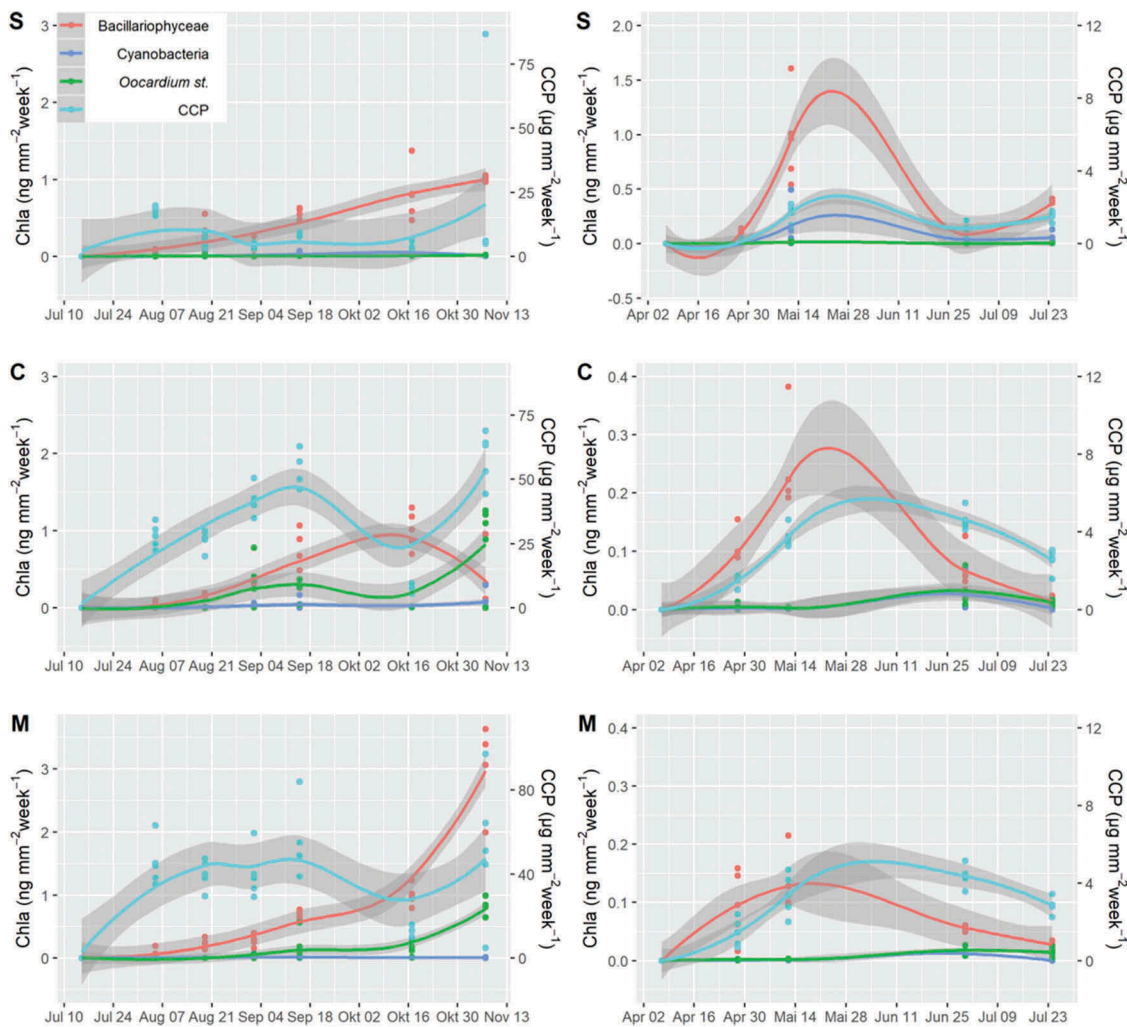
Fig. 20. Predicted biofilm development calculated separately for the sites S (spring), C (centre) and M (mouth) and years 2008 and 2009.

During periods of low discharge combined with high irradiance, diatom mats developed thick, brownish, mucous-like coatings. At site S, CCP precipitation might have been too low to result in a competitive advantage for *O. stratum*; thus cyanobacteria and heterotrophic bacteria dominated (Fig. 20). Our results indicated a spatial-temporal niche differentiation for *O. stratum* and cyanobacteria. While cyanobacteria were greater at site S and during spring, *O. stratum* developed best at site C during late summer and late autumn (Fig. 20). In contrast, diatoms were linked neither to spatial (site) nor to temporal (season) factors. Except for site M during late autumn, this group dominated the photoautotrophic biofilm (Table S5), which agrees with Zancarini *et al.* (2017).

Colonies of *O. stratum* were macroscopic along a certain stretch downstream from where SAL precipitation started. This pattern was observed in former studies (Linhart & Schagerl 2015; Rott *et al.* 2010; Wallner 1934), but the reasons for this were unclear. Our survey suggests that very specific abiotic conditions are fundamental for the occurrence of this desmid. If these criteria are met, biotic interactions come into play. Consumers like ciliates, flagellates, nematodes and young instar insects are apparently not a critical factor, as we did not find feeding traces. We assume that calcification of colonies acts as protection against grazing.

Schagerl & Wukovits (2014) revealed in a culture that *O. stratum* does not use HCO_3^-, but has very efficient carbon dioxide uptake. The cultures showed high production of extracellular polymeric substances and a patchy growth pattern in hemispherical colonies, but without carbonate precipitation. This points to mainly abiotic calcification in its natural environment. The stalks promote calcite nucleation in HCO_3^- and Ca^{2+} oversaturated waters, thus increasing CCP (see Merz-Preiß & Riding 1999; Pentecost 1985). High amounts of CCP requires *O. stratum* to develop stalks in order to prevent carbonate covering. Higher abiotic precipitation, therefore, leads to increased excretion of extracellular polymeric substances and vice versa. As a consequence, the biomass of *O. stratum* is very likely regulated by the amount of CCP.

ACKNOWLEDGEMENTS

REFERENCES

Battin T., Kaplan L., Newbold J., Cheng X. & Hansen C. 2003. Effects of current velocity on the nascent architecture of stream microbial biofilms. *Applied and Environmental Microbiology* 69: 5443–5452. DOI: 10.1128/AEM.69.9.5443-5452.2003.

Bazylinski D.A. 2003. Biologically controlled mineralisation in prokaryotes. *Reviews in Mineralogy and Geochemistry* 54: 217–247. DOI: 10.2113/0540217.

Besemer K., Singer G., Limberger R., Chlup A.-K., Hochedlinger G., Hödl I., Baranyi C. & Battin T.J. 2007. Biophysical controls on community succession in stream biofilms. *Applied and Environmental Microbiology* 73: 4966–4974. DOI: 10.1128/AEM.00588-07.

Bosellini A., Gianolla P. & Stefani M. 2003. Geology of the Dolomites. *Episodes* 26: 181–185.

Breusch T.S. & Pagan A.R. 1979. A simple test for heteroscedasticity and random coefficient variation. *Econometrica* 47: 1287–1294. DOI: 10.2307/1911963.

Brotas V. & Plante-Cuny M.R. 2003. The use of HPLC pigment analysis to study microphytobenthos communities. *Acta Oecologica* 24: 109–S115. DOI: 10.1016/S1146-609X(03)00013-4.

Burns A. & Walker K. 2000. Effects of water level regulation on algal biofilms in the River Murray, South Australia. *Regulated Rivers: Research and Management* 16: 433–444. DOI: 10.1002/1099-1646(200009/10)16:5<433::AID-RRR595>3.0.CO;2-V.

Cantonati M., Segadelli S., Ogata K., Tran H., Sanders D., Gerecke R., Rott E., Filippini M., Gargini A. & Celico F. 2016. A global review on ambient limestone-precipitating springs (LPS): hydrogeological setting, ecology, and conservation. *Science of the Total Environment* 568: 624–637. DOI: 10.1016/j.scitotenv.2016.02.105.

Dittrich M. & Sibler S. 2010. Calcium carbonate precipitation by cyanobacterial polysaccharides. *Geological Society, London, Special Publications* 336: 51–63. DOI: 10.1144/SP336.4.

Domozych D.S. & Domozych C.R. 2008. Desmids and biofilms of freshwater wetlands: development and microarchitecture. *Microbial Ecology* 55: 81–93. DOI: 10.1007/s00248-007-9253-y.

Dupraz C., Reid R.P., Braissant O., Decho A.W., Norman R.S. & Visscher P.T. 2009. Processes of carbonate precipitation in modern microbial mats. *Earth-Science Reviews* 96: 141–162. DOI: 10.1016/j.earscirev.2008.10.005.

Faupl P. 2003. *Historische Geologie: eine Einführung*, ed. 2. UTB, Stuttgart, Germany. 272 pp.

Field C.B. 1998. Primary production of the biosphere: integrating terrestrial and oceanic components. *Science* 281: 237–240. DOI: 10.1126/science.281.5374.237.

Golubić S. & Marčenko E. 1958. Zur Morphologie und Taxonomie der Desmidiaceengattung. *Oocardium. Schweizerische Zeitschrift für Hydrologie* 20: 177–185.

Linhart C. & Schagerl M. 2015. Seasonal succession of the travertine-forming desmid *Oocardium stratum*. *Journal of Phycology* 51: 1055–1065. DOI: 10.1111/jpy.12345.

Mackey M.D., Higgins H.W., Mackey D.J. & Wright S.W. 1997. CHEMTAX user's manual: a program for estimating class abundances from chemical markers – application to HPLC measurements of phytoplankton pigments. *Report 229*. 41 pp.

Martinez R.E., Gardés E., Pokrovsky O.S., Schott J. & Oelkers E.H. 2010. Do photosynthetic bacteria have a protective mechanism against carbonate precipitation at their surfaces? *Geochimica et Cosmochimica Acta* 74: 1329–1337. DOI: 10.1016/j.gca.2009.11.025.

Merz-Preiß M. & Riding R. 1999. Cyanobacterial tufa calcification in two freshwater streams: ambient environment, chemical thresholds and biological processes. *Sedimentary Geology* 126: 103–124. DOI: 10.1016/S0037-0738(99)00035-4.

Pentecost A. 1985. Association of cyanobacteria with tufa deposits: identity, enumeration, and nature of the sheath material revealed by histochemistry. *Geomicrobiology Journal* 4: 285–298. DOI: 10.1080/01490458509385936.

Pentecost A. 1991. A new and interesting site for the calcite encrusted desmid *Oocardium stratum* Naeg. in the British Isles. *British Phycological Journal* 26: 297–302. DOI: 10.1080/00071619100650261.

Pentecost A. 2005. *Travertine*. Germany, Springer, Berlin. 446 pp.

R Core Team. 2018. *R: a language and environment for statistical computing*. R Foundation for Statistical Computing, Vienna.

Ramette A. 2007. Multivariate analyses in microbial ecology. *FEMS Microbiology Ecology* 62: 142–160. DOI: 10.1111/j.1574-6941.2007.00375.x.

Roberts S., Sabater S. & Beardall J. 2004. Benthic microalgal colonization in streams of differing riparian cover and light availability. *Journal of Phycology* 40: 1004–1012. DOI: 10.1111/j.1529-8817.2004.03333.x.

Roeselers G., Van Loosdrecht M.C.M. & Muyzer G. 2007. Heterotrophic pioneers facilitate phototrophic biofilm development. *Microbial Ecology* 54: 578–585. DOI: 10.1007/s00248-007-9238-x.

Rott E., Holzinger A., Gesierich D., Kofler W. & Sanders D. 2010. Cell morphology, ultrastructure, and calcification pattern of *Oocardium stratum*, a peculiar lotic desmid. *Protoplasma* 243: 39–50. DOI: 10.1007/s00709-009-0050-y.

Sabater S., Gregory S.V. & Sedell J.R. 1998. Community dynamics and metabolism of benthic algae colonizing wood and rock substrata in a forest stream. *Journal of Phycology* 34: 561–567. DOI: 10.1046/j.1529-8817.1998.340561.x.

Sanders D. & Rott E. 2009. Contrasting styles of calcification by the micro-alga *Oocardium stratum* Naegeli 1849 (Zygnematophyceae) in two limestone-precipitating spring creeks of the Alps. *Austrian Journal of Earth Sciences* 102: 34–49.

Sanders D., Wertl W. & Rott E. 2010. Spring-associated limestones of the Eastern Alps: overview of facies, deposystems, minerals, and biota. *Facies* 57: 395–416. DOI: 10.1007/s10347-010-0252-y.

Schagerl M. & Donabaum K. 2003. Patterns of major photosynthetic pigments in freshwater algae. 1. Cyanoprokaryota, Rhodophyta and Cryptophyta. *Annales de Limnologie - International Journal of Limnology* 39: 35–47. DOI: 10.1051/limn/2003003.

Schagerl M. & Pröschold T. 2007. Rediscovery of *Oocardium stratum* Naeg. in Austria and its preliminary taxonomic position within the Desmidiales. *In: Proceedings - Biology and Taxonomy of Green Algae V. Smolenice-Castle.*

Schagerl M. & Wukovits J. 2014. Cultivation and inorganic carbon uptake of the rare desmid *Oocardium stratum* (Conjugatophyceae). *Phycologia* 53: 320–328. DOI: 10.2216/13-228.1.

Schlüter L., Møhlenberg F., Havskum H. & Larsen S. 2000. The use of phytoplankton pigments for identifying and quantifying phytoplankton groups in coastal areas: testing the influence of light and nutrients on pigment/chlorophyll *a* ratios. *Marine Ecology Progress Series* 192: 49–63. DOI: 10.3354/meps192049.

Stolz J.F. 2000. Structure of microbial mats and biofilms. In: *Microbial sediments* (Ed. by R.E. Riding & S.M. Awramik), pp. 1–8. Springer, Berlin, Heidelberg, Germany. 331 pp.

Strahler A.N. 1957. Quantitative analysis of watershed geomorphology. *Eos, Transactions American Geophysical Union* 38: 913–920. DOI: 10.1029/TR038i006p00913.

Talling J.F. & Driver D. 1963. Some problems in the estimation of chlorophyll *a* in phytoplankton. In: *Proceedings of the conference on primary productivity measurement, marine, freshwater*. University of Hawaii, Honolulu, Atomic Energy Commission TID-7633, 142–146 pp.

Trobej M., Bednar J., Waringer J. & Schagerl M. 2017. Algal communities of spring-associated limestone habitats. *Aquatic Microbial Ecology* 80: 61–75. DOI: 10.3354/ame01836.

Van Den Meersche K., Soetaert K. & Middelburg J.J. 2008. A Bayesian compositional estimator for microbial taxonomy based on biomarkers. *Limnology and Oceanography Methods* 6: 190–199. DOI: 10.4319/lom.2008.6.190.

Vannote R.L., Minshall G.W., Cummins K.W., Sedell J.R. & Cushing C.E. 1980. The river continuum concept. *Canadian Journal of Fisheries and Aquatic Sciences* 37: 130–137. DOI: 10.1139/f80-017.

Wallner J. 1933. *Oocardium stratum* Naeg., eine wichtige tuffbildende Alge Südbayerns. *Planta* 20: 287–293. DOI: 10.1007/BF01909569.

Wallner J. 1934. Über die Verbreitungsökologie der Desmidiacee *Oocardium*. *Planta* 23: 249–263. DOI: 10.1007/BF01925450.

Wallner J. 1935. Eine gesteinsbildende Süßwasser-Alge Deutschlands. *Natur und Volk* 66: 85–91.

Weiner S. 2003. An overview of biomineralization processes and the problem of the vital effect. *Reviews in Mineralogy and Geochemistry* 54: 1–29. DOI: 10.2113/0540001.

Wright S.W., Jeffrey S.W., Mantoura R.F.C., Llewellyn C.A., Bjørnland T., Repeta D. & Welschmeyer N. 1991. Improved HPLC method for the analysis of chlorophylls and carotenoids from marine phytoplankton. *Marine Ecology Progress Series* 77: 183–196. DOI: 10.3354/meps077183.

Zancarini A., Echenique-Subiabre I., Debroas D., Taïb N., Quiblier C. & Humbert J.F. 2017. Deciphering biodiversity and interactions between bacteria and microeukaryotes within epilithic biofilms from the Loue River, France. *Scientific Reports* 7: 4344. DOI: 10.1038/s41598-017-04016-w.

Zhu T. & Dittrich M. 2016. Carbonate precipitation through microbial activities in natural environment, and their potential in biotechnology: a review. *Frontiers in Bioengineering and Biotechnology* 4: 4. DOI: 10.3389/fbioe.2016.00004.

Zuur A.F., Ineo E.N., Walker N.J., Saveliev A.A. & Smith G.M. 2009. *Mixed effects models and extensions in ecology with R*. Springer, New York, United States. 574 pp.